NANO LETTERS

pubs.acs.org/NanoLett Letter

Spatially Resolved Nonlinear Plasmonics

Johannes Schust,*,# Florian Mangold,# Florian Sterl, Niklas Metz, Thorsten Schumacher, Markus Lippitz, Mario Hentschel, and Harald Giessen*

Cite This: *Nano Lett.* 2023, 23, 5141−5147 Read Online

ACCESS | Metrics & More | Article Recommendations | Supporting Information

ABSTRACT: Nonlinear optical plasmonics investigates the emission of plasmonic nanoantennas with the aid of nonlinear spectroscopy. Here we introduce nonlinear spatially resolved spectroscopy (NSRS) which is capable of imaging the k-space as well as spatially resolving the THG signal of gold nanoantennas and investigating the emission of individual antennas by wide-field illumination of entire arrays. Hand in hand with theoretical simulations, we demonstrate our ability of imaging various oscillation modes inside the nanostructures and therefore spatial emission hotspots. Upon increasing intensity of the femtosecond excitation, an individual destruction threshold can be observed. We find certain antennas becoming exceptionally bright. By investigating those samples taking structural SEM images of the nanoantenna arrays afterward, our spatially resolved nonlinear image can be correlated with this data proving that antennas had deformed into a peanut-like shape. Thus, our NSRS setup enables the investigation of a nonlinear self-enhancement process of nanoantennas under critical laser excitation.

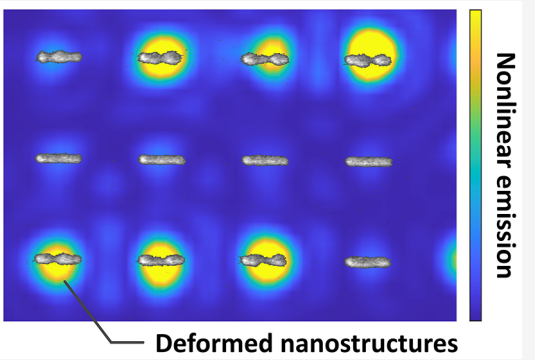

KEYWORDS: *Nanoantennas, Plasmonics, Imaging, Third Harmonic Generation, Self-enhancement*

Nonlinear optical properties of plasmonic nanostructures[1] have attracted attention in recent years, as it is certain that the local enhancement of the optical field can cause highly nonlinear effects inside the structures. This in turn, in combination with suitable nonlinear materials, would then funnel the fundamental light into the nonlinear optical hot spots, which then might emit nonlinear radiation. This could include not only second- or third-harmonic light;[2−5] also sum- or difference-frequency generated light, four-wave mixing, or optical rectification processes might be favorably enhanced. Subsequently, using optical nanoantennas for boosting the re-radiation of the light that was generated by this nonlinear optical process, extremely high absolute nonlinear optical efficiencies might be obtained.[6−10] As nonlinear optical materials, polymers,[11] semiconductors such as quantum wells and quantum dots,[7] dielectrics such as ITO,[2,8] along with gold itself which has a quite high optical nonlinearity might be used.[8,12−14]

Key to high nonlinear conversion efficiency is the exact knowledge of the spatial, spectral, and temporal/phase properties of the local optical light fields. Different attempts to control[15] and to measure these properties have been reported.[16−18] For example, Hanke et al.[19] scanned a variety of nanostructures such as double dots, double ellipses, and rods with a gap through the focus of a femtosecond laser beam and recorded the third-harmonic generation (THG) intensity as a function of laser focus position. They also investigated the dependence of that nonlinear light intensity as a function of shape and found that extremely elongated shapes are beneficial for THG efficiency. However, they did not image the entire structure under light illumination, and they did not detune the exciting laser with respect to the plasmonic resonances. Aeschlimann et al. carried out spatiotemporal as well as phase pulse shaping to control the emission of light from plasmonic oligomers.[20] They utilized photoemission electron microscopy (PEEM) to analyze the spatial origin of the light emission. In the work by Wolf et al.,[17] k-space imaging was utilized, which revealed the directionality of the emitted THG light. Kauranen and Zayats, Chen et al., Drechsler et al., Krauth et al., Metzger et al., and Wegener et al.[1,21−25] have studied second-harmonic generation (SHG) and THG emission of plasmonic nanostructures depending on shape, material, spectral detuning, pulse duration, etc. However, in most of those cases, the local microscopic origin was also not spatially imaged but mostly derived by using linear or nonlinear optical simulations. Butet and Martin analyzed the mode structure of SHG light in plasmonic gold rods and dimers.[26]

Here, we thus introduce a *spatially and spectrally* resolved nonlinear microscopic imaging technique which allows us to study plasmonic nanostructures and their nonlinear optical

Received: March 20, 2023
Revised: May 16, 2023
Published: May 24, 2023

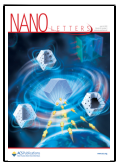

https://doi.org/10.1021/acs.nanolett.3c01070
Nano Lett. 2023, 23, 5141−5147

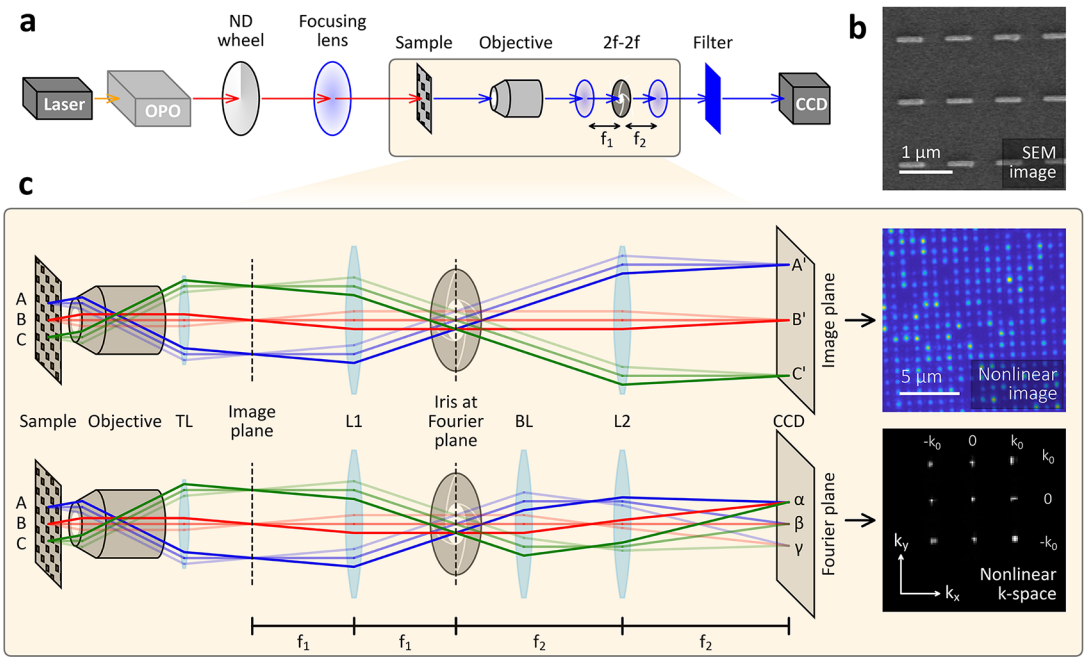

Figure 1. Schematic setup in (a) provides the possibility to focus pulsed laser light at different wavelengths onto a sample. As shown in the SEM image in (b), we use arrays of plasmonic rod antennas. Resonances inside the nanorods lead to nonlinear effects such as third-harmonic generation. The according emission pattern can be imaged with the help of a 2f−2f microscopy setup combined with a CCD camera. The microscope uses a 100× objective as well as a corresponding tube lens (TL) that collect the hitherto infinity corrected beams. The detailed insight (c) depicts the 2f−2f setup, consisting of two imaging lenses of different focal lengths f1 and f2. The measurements on the right in (c) demonstrate that we can individually distinguish between single antennas and their nonlinear emission hotspots. Irregularities like those are a suitable way to characterize the resolution of the setup and its ability to identify single exceptionally bright or dark emission hotpots or even missing plasmonics. Fourier space measurements are possible, as well, by adding a so-called Bertrand lens.

emission, in our case for THG of gold nanoantennas. We illuminated an *entire array* of nanostructures simultaneously via our wide-field illumination setup and image the nonlinear response. In addition, we characterize the nanostructures carefully with respect to their spectral response, and we have the ability to spectrally tune our optical parametric femtosecond laser source over the plasmonic resonances. By investigating those samples by taking SEM images, our method allows for correlated structural and nonlinear optical measurements that might lead to improved antenna shapes in the future with extremely high nonlinear conversion properties.

Figure 1a gives an overview of the setup. As pump laser, we use an Yb:KGW solid state laser that has an average output power of about 2.1 W, a repetition rate of 44 MHz, a wavelength of 1025 nm, and a pulse duration of approximately 170 fs. The laser beam (orange arrow) passes through a fan-out nonlinear periodically poled lithium niobate (PPLN) crystal placed inside a fiber-feedback optical parametric oscillator (OPO).[27] In that way we are achieving laser pulses that exhibit a tunable wavelength range in the near-infrared from about 1300 to 1900 nm, appearing with averaged output power of up to 550 mW (red arrows). To adjust power and focus position, the laser beam passes through a continuous ND filter wheel and a focusing lens. If the sample is placed at the focal point (beam waist approximately 15 μm) of the lens, very high local and temporal peak intensities of up to 70 GW/cm^2 can be achieved. Such high power induces nonlinear effects on the sample, which generate light at a different wavelength (blue arrows).

A scanning electron microscope (SEM) image of a typical sample is shown in Figure 1b. Gold nanoantennas are arranged in lattices to enhance the linear response. Typical dimensions are equal thickness and width of 50 nm, length of 400 nm, and periodicity of about 1000 nm. When exciting resonances inside the nanorod, nonlinear optical effects occur. We are particularly interested in THG, exhibiting a three times shorter wavelength than the corresponding linear response. Such nonlinear emission patterns can now be analyzed using our technique of spatial imaging.

To efficiently collect the nonlinear signal, a 100× objective of numerical aperture (NA) 0.9 is placed directly behind the sample. Focusing is assisted by a feedback-controlled high-precision piezo stage with 0.1 nm resolution. Figure 1c depicts the detailed beam paths of our two imaging modes. The upper part illustrates real space imaging, while the lower part shows our possibility to access the k-space. An explicit explanation is given in the Supporting Information. The switching between real-space and Fourier imaging obtained by the 2f−2f setup, as well as the iris at the accessible Fourier plane, allow one to induce controlled manipulation of the nonlinear image by cropping single k-space orders. The corresponding effects are mainly used for characterizing various imaging artifacts, as demonstrated in Figure S1. The nonlinear emission is small compared to the remaining signal and the linear response of the sample. To obtain exclusively the nonlinear signal, optical filters are placed directly in front of the CCD camera at the back focal plane. For our highly sensitive measurements, we use a combination of a PIXIS 256E camera and a SP2500 spectrometer from Princeton Instruments, easily allowing switching between the imaging and spectroscopy mode just by rotating an optical grating from first to zeroth order.

https://doi.org/10.1021/acs.nanolett.3c01070
Nano Lett. 2023, 23, 5141−5147

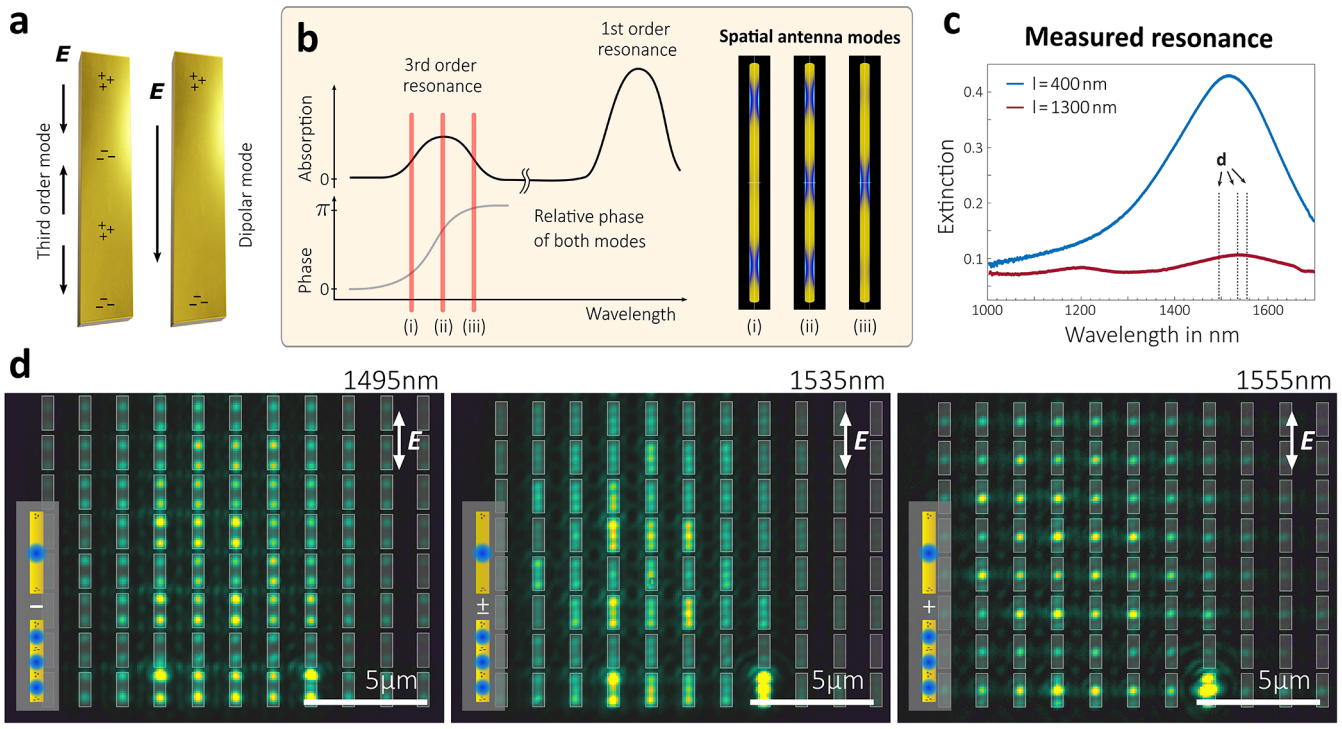

Figure 2. In a nanorod, different plasmon oscillations arise. They are characterized by electric field and charge density, as graphically illustrated in (a). The resonance spectrum of a gold nanorod consists of various resonance peaks. (b) The dominant one is the first-order resonance with the trivial dipolar mode predominating. At shorter wavelengths, the third-order resonance can be observed, consisting of coexisting dipolar and third-order oscillation mode. Constructive or destructive interference, depending on their changing relative phase, governs this process. The images on the right in (b) are the results of FEM simulations, that confirm the strongly wavelength-dependent THG emission. Depending on the exact spectral position on the resonance, different spatial emission modes arise, as depicted in blue on the gold nanoantennas. (c) Linear plasmonic extinction using FTIR extinction measurements (blue: antenna length 400 nm, red: antenna length 1300 nm). Third-order mode excitation was realized by switching to three times longer antennas, with the third-order resonance situated around 1535 nm. (d) Spatial nonlinear THG emission around 512 nm when exciting the nanoantenna array. The fundamental wavelength is tuned over the third-order resonance peak. The coexistence of the differently interfering modes, as illustrated in the insets, can be directly imaged.

A typical real-space measurement result is depicted on the right in Figure 1c. We excite the antenna lattice resonantly and image the emerging nonlinear signal. A color-map indicates the strength of the imaged THG signal with spatial resolution in the $x-y$ direction. The yellow hotspots correspond to the nonlinear emission centers of the nanoantennas. Revealing all the spatial artifacts, this method grants new opportunities to study the nonlinear resonance properties of nanoantennas. Irregularly bright antennas can be identified. The k-space measurement exposes the periodicity of the emission and can be analyzed for optimizing accuracy and avoiding systematic imaging faults such as low-pass filter effects.

For a correct interpretation of the generated images, an understanding of the nonlinear emission pattern of nanoantennas is fundamental. The exact location of the single emission hotspots goes along with the internal electric field inside the nanostructures. Due to this fact, the common emission in dipolar oscillation is located in the center of the antennas. Additionally, far-field imaging of further resonances inside the antennas is proven possible. Slightly varied parameters, exemplary excitation wavelength, are able to fundamentally change the distribution of emission hotspots, as it was analogously discussed using k-space studies.[17]

Beside the common dipolar resonance, we are dealing with the instance of a higher mode resonance, namely, third-order, since the second-order excitation is dipole-forbidden.[28] The according modes are characterized by different charge oscillations and THG emission hotspots that are illustrated in Figure 2a. As demonstrated in the schematic spectrum in Figure 2b, the third-order resonance peak is positioned at much shorter wavelengths. To obtain a sufficiently large nonlinear response, separate nanoantenna lattices with adjusted configurations have been manufactured. Consisting of significantly longer antennas arranged in according arrays, we shift the resonance up to the working region of our OPO (1300−1900 nm). Linear extinction measurements performed by an Fourier transformation infrared (FTIR) spectrometer are plotted in Figure 2b and indicate that the peak of the first-order resonance of common short antennas exhibits a nice accordance to the spectral position of the third-order peak of three times longer ones. However, the latter gives only poor linear response, which makes excitation of the localized surface plasmons difficult. To overcome this, we are using the highest available incident laser power for our spatially resolved nonlinear measurements, reaching up to about 550 mW.

Additionally, Figure 2b depicts the relative phase between first- and third-order mode, which is a crucial parameter for further imaging studies as well. When changing the incident driving frequency, the plasmonic response of the material performs a phase shift of π at the resonance peak. Since we are exciting the third-order resonance, this phase shift affects this mode exclusively and its relative phase to the coexisting dipolar mode changes. The coexistence of the two oscillation modes leads to interference effects. If the phase difference between the

https://doi.org/10.1021/acs.nanolett.3c01070
Nano Lett. 2023, 23, 5141−5147

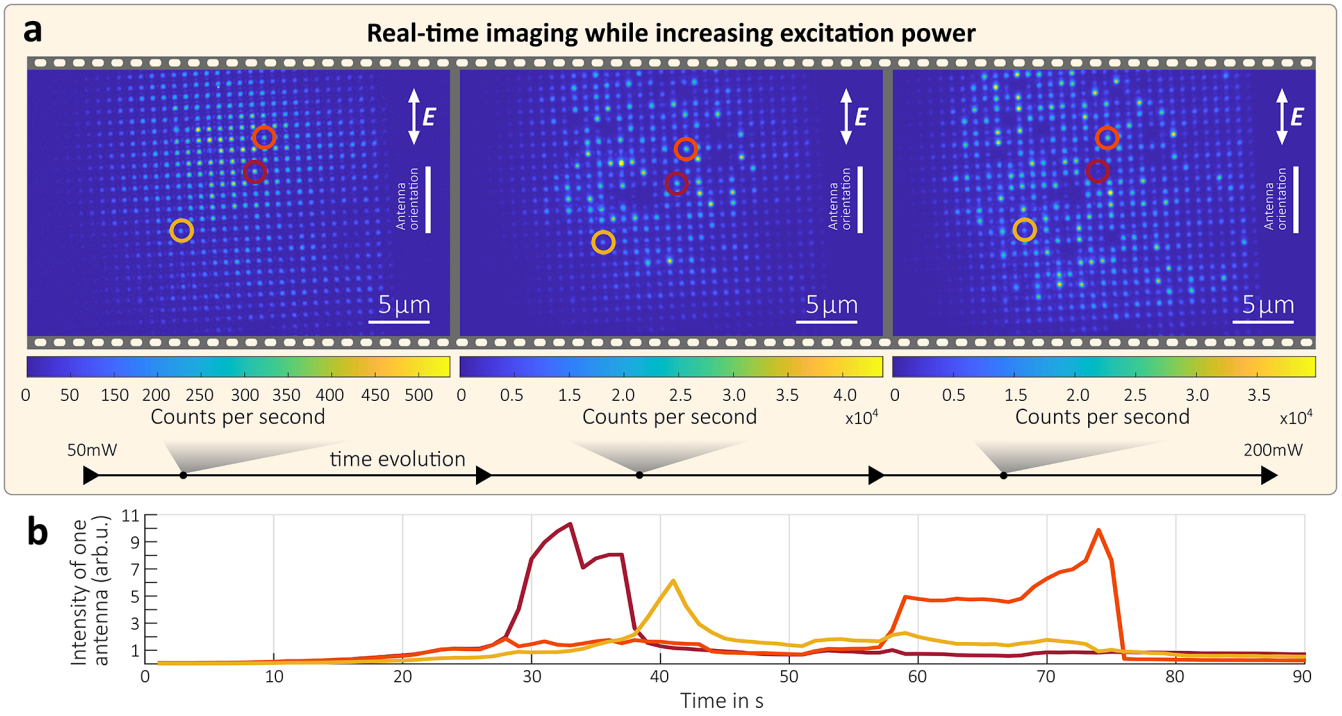

Figure 3. Before breaking, the individual plasmonic structures exhibit unexpected behavior. (a) Spatial images of the nanoantennas nonlinear emission upon overexcitation are depicted. They are excerpts of a time-resolved measurement of in total 90 s, while for each image the THG signal was integrated for 1 s. During the measurement, the excitation power was persistently increased. The spatial Gaussian beam profile governs this measurement. In addition to a collectively rising emission, single antennas are further enhancing their intensity at critical excitation. This effect remains concealed when not evaluating spatial images but only looking at the total emitted intensity. The measurement was carried out resonantly at 1535 nm and up to a laser power of 200 mW. Antennas of width 50 nm and length 400 nm are used. The temporal trend of the emission intensity of some single, exemplary marked nanoantennas is extracted and plotted in (b).

first-order and the third-order oscillation vanishes, the central emission hotspot is governed by destructive interference. The according emission hotspot cancels out. For constructive interference, the electric field vector positioned in the middle of the antenna at third-order oscillation mode is parallel to the one in dipolar mode, which is given at an overall phase difference of π. In this regime, the central hotspot dominates the THG emission. However, exactly at resonance, the three hotspots can be spatially observed with approximately equal intensity. Our simulation show good accordance with this intuitive explanation. The corresponding results are depicted next to the schematic spectrum and show data for three spectral positions of interest.[17]

Three different spatially resolved measurements of the third-order resonances of antennas with length 1300 nm are depicted in Figure 2d. The wavelength is chosen to be positioned below (1495 nm), at (1535 nm), and above (1555 nm) the third-order resonance peak, as also indicated in (b). Slight changes of the excitation wavelength change the detected spatial THG emission fundamentally. This behavior is originated in the occurrence of both the dipolar oscillation mode and the third-order mode, simultaneously. The insets are again accentuating the simplified model given above. Dipolar and third-order oscillation modes in either constructive (+) or destructive (−) coexistence, dependent on their relative phase, are merging into the measured emission pattern. Our measurements jointly with the spatial simulations not only prove the functionality of the setup; this wide-field imaging also opens up a chance for experimental verification of theoretical studies concerning charge configuration and electric fields, even in more complex nanostructures.

Regarding the high power density focused on the sample, it is crucial to investigate the excitation threshold of the plasmonic nonlinear optical efficiency in more detail. Insights into spatial information can now be gained using our imaging technique. Since we are able to choose a suitable lattice constitution with high nonlinear response, it does further allow a real-time observation of the THG emission. We are able to reduce the integration time of the CCD camera below 1 s. Reaching an excitation threshold of the nanoantennas, such time-resolved imaging becomes necessary due to a dynamic evolution of the nanoantennas response. When the nanoantennas are close to their destruction threshold, their THG emission was found to exhibit unexpected features, which would remain hidden without spatial imaging.

Figure 3a plots three excerpts of time-resolved measurements. The measurements were performed to execute a controlled intensity increase of the nanoantenna lattices. During this destructive process, single antennas exhibit extremely nonlinear behavior. The THG image of Figure 3a proves reproducible bright THG generation of the antennas at a critical excitation level. The images are dominated by a Gaussian laser beam profile. As expected, the interesting effects are first detected in the center, where the power density is highest. In this specific measurement, the incident laser intensity is increased in a range between 50 mW and 200 mW. As one can see, nearly every antenna is enhancing its nonlinear light emission intensity significantly before it becomes dark, while the exact moment is randomly spread

https://doi.org/10.1021/acs.nanolett.3c01070
Nano Lett. 2023, 23, 5141−5147

over several seconds. The time-spread conceals this novel effect when doing common measurements of total signal intensities without spatial resolution. Exemplarily, three different antenna intensities were plotted as a function of measurement time in Figure 3b. The according antennas are additionally identified with red, orange, and yellow circles. The three evaluated antennas show the mentioned behavior noticeably in the plots. Their individual total intensity is increasing, followed by a short plateau at a high nonlinear signal level. Afterward, the THG intensity drops again and the antenna becomes dark. This transitory effect showing up at a precise destruction has not been reported before, to the best of our knowledge. We observe only a few individual antennas that become dislocated by peeling off the substrate. In our THG measurements, they can be seen as instantly vanishing emission hotpots. These antennas are probably affected by imperfections in the production process, reducing their stability. A video of the data can be accessed in the Supporting Information. The process of destruction with the two temporal regimes of THG emission enhancement and the subsequent vanishing of the emission can be interrupted at any time by stopping the excitation momentarily. Proceeding in that way, the achieved emission pattern freezes directly in the current constitution. Followed by an excitation with lower intensities far beneath the critical limit, it is possible to retain the THG efficiencies and further analyze the plasmonics nanostructures. The bright antennas maintain their emission properties. However, the already dark ones remain permanently destroyed.

Microscopic insight can be achieved by the use of scanning electron microscopy (SEM). The measured THG emission can be studied and compared to the actual plasmonic structures, in order to find the origin for the unusual detected high nonlinear signal. Figure 4a shows a correlation of SEM image and THG measurement. The latter relies on a targeted manipulation of the structures. Therefore, the incident laser is precisely focused on single antennas to evoke the brightest possible emission hotspot. Adjusting laser power, the width of the focal point and its position offer a chance to roughly pick out an individual antenna to reach a critical nonlinearity. The procedure was stopped right before the plasmonic emission ceases to exist. The exact moment is not easy to predict, since every antenna acts individually. The superimposed THG image in Figure 3a is an interpolated measurement at an incident wavelength of 1550 nm. The outstanding antennas with high THG emission manifest themselves as the extremely bright yellow spots. They are surrounded by unaffected antennas, as they are still in their initial shape as produced. Antennas that show the essential enhancement of their emission do all have a similar shape like a peanut. Their gold material is rearranged, so they now exhibit a smaller, strangulated waist and thicker ends. *The antennas run through a self-induced shape transformation, adjunct to a nonlinear efficiency enhancement.* This is taken to the extreme until the connection in the middle is severed and the structure separates into two dots. One can also observe this case in the right excerpt of Figure 4a, where an antenna that has already lost its nonlinear response is marked in red. Its resonance is now shifted far away to different wavelengths, so we do not record any nonlinear response anymore. This "peanut" shape transformation process is seemingly reproducible.

Further, the resonance spectrum of these single antennas is evaluated in Figure 4b. The plot depicts the THG emission in dependence of the fundamental wavelength of the incident laser beam. The single-antenna intensity was extracted from

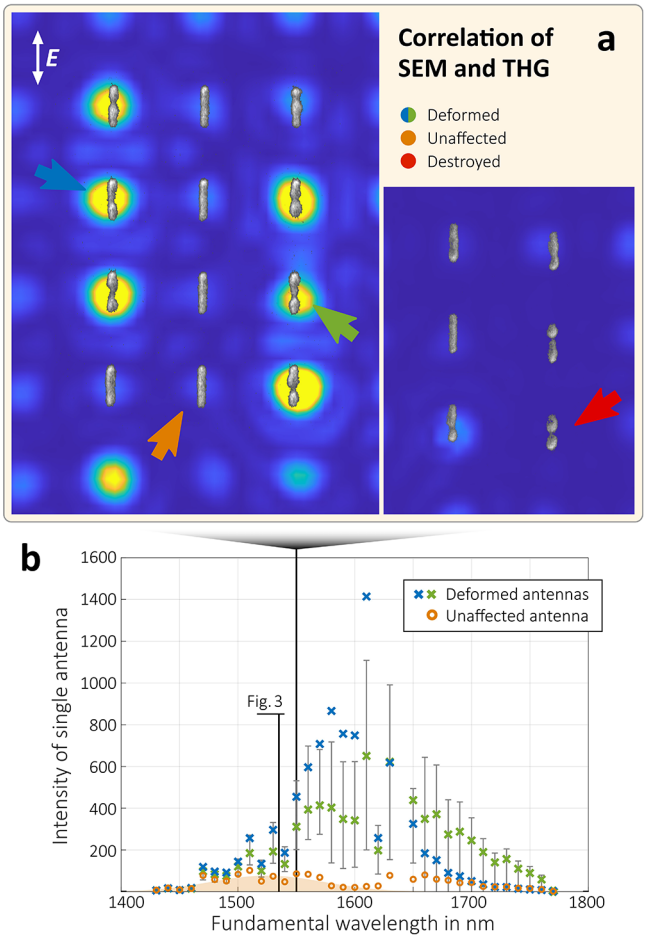

Figure 4. Scanning electron microscopy (SEM) allows the correlation of these unusual THG properties with the actual shape of the antennas. (a) Interpolated THG emission measurement at a fundamental wavelength of 1550 nm, where the antennas were previously exposed to trigger the highest THG efficiency possible. Two different sections of the sample are displayed (left: 4 × 3 antennas, right: 3 × 2 antennas). The superimposed SEM images depict a self-induced, reproducible deforming of the nanorods, while destroyed antennas sever into two dots. Examples for antennas with different properties are marked with arrows. As seen in a spatial evaluation of the spectrum (b) of the single antennas, their nonlinear resonance is both red-shifted and enhanced. For comparison, the spectrum of an unaffected nanoantenna is plotted as well. The second peak at 1650 nm stems from systematic imaging errors due to low-pass filter effects. The error bars are representing the intensity standard deviation of the evaluated antennas. The spectral imaging position of the THG measurements of (a), as well as of Figure 3, is marked in the plot.

the raw data of the CCD chip by integrating over the area of one antenna, while paying attention to slight shifts caused by dispersion. It is noteworthy that the combination of spectral and spatial evaluation comes with several difficulties to consider. An example for such a systematic error is the second peak in the spectrum of the unaffected antenna, which is originated in some remaining low-pass filter oscillations that have been numerically evaluated. Spatial artifacts of the bright dots are able to conceal the comparably small emission centers in the surroundings. The maximum intensity of the different enhanced sites cannot be predicted quantitatively until now. The error-bars show the standard deviation, while they are positioned around the mean intensity of the six antennas. For

https://doi.org/10.1021/acs.nanolett.3c01070
Nano Lett. 2023, 23, 5141−5147

demonstration purposes, explicit values of three highlighted antennas were also plotted and marked with green and blue indicators. In addition to the much higher resonance, we observe a significant red shift of the THG emission spectrum. The maximum is positioned at a fundamental wavelength in the range of about 1590 to 1620 nm. The width of the deformed antenna resonance covers the original peak, too. Hence, the enhancement we see in Figure 3a is just due to an off-resonant response of the deformed antennas. The deformation most likely originates from heat generation of the plasmonics due to the resonance in the femtosecond time domain. Such local heating processes were previously modeled,[29−31] and self-optimization processes of plasmonics due to strong electric fields have been identified, too.[32] We suppose that this self-modification of the antennas encourages the emission into the far field. First simulations reveal that the resulting shape of the modified antennas is a more suitable resonator for the emerging THG wavelengths. Analogously to already investigated bow-tie antennas,[33] that partly resemble the observed deformed shape, this could be one reason for the observed enhancement.

In summary, we carried out spatially resolved imaging of nonlinear plasmonics and gained several new insights. By analyzing the nonlinear emission distributions inside the antenna, we observed a strong dependence on the spectral position of the pump laser relative to the antenna resonance. Especially when dealing with third-order resonance, we obtain either one, two, or three emission hotspots per antenna. Different emission patterns originate from the coexistence of the first- and third-order resonance modes. Their varying relative phase specifies whether interference is occurring in a constructive or destructive fashion. In the spectral region around the third-order resonance peak of the structures, the phase changes by a value of π; thus a fundamental change in the nonlinear emission occurs.[17] Understanding these effects grants new opportunities to influence the nonlinear far-field and study the field distributions in plasmonic nanostructures. We further studied the nonlinear spatial behavior of antenna arrays upon increasing pump laser intensity. When carrying out time-dependent measurements on a level of seconds, we discovered an unexpected critical behavior of single antennas before breaking. The individual antennas enhance their THG emission for several seconds. A correlation of this increasing THG efficiency with the actual microscopic structure shows a reproducible change of shape of the abnormally bright antennas. A deformation of the gold material to a peanut shape is observed. This self-configuration can be triggered by precise overexcitation to yield the highest possible nonlinear response.

Further simulations could verify our hypothesis for the origin of the plasmonic deformation. A profound understanding of acting forces and currents inside the gold material, as well as local heating and melting in the femtosecond time domain, is inevitable for explaining such novel effects at critical excitation. Further, the increasing THG efficiency can be explained by these methods. A deeper insight into the individual behavior of plasmonic nanoantennas can offer opportunities to systematically increase their third-harmonic response. Such can be done either directly in the production process or afterward as a postprocessing of the sample using well-defined laser treatment. Using the common fabrication technology of electron beam lithography it is possible to obtain nearly every shape of nanostructure. By varying different parameters, artificially deformed antennas in that observed peanut shape can be produced. THG intensity measurements can give information about the emission properties and allow a subsequent comparison. Exaggerating structure characteristics that show high nonlinear intensities can lead to iteratively improved nonlinear nanoantennas.

■ ASSOCIATED CONTENT

Supporting Information

The Supporting Information is available free of charge at https://pubs.acs.org/doi/10.1021/acs.nanolett.3c01070.

Detailed description of the imaging principle using both real-space and Fourier imaging, as well as an examplary characterization of possible imaging artifacts (PDF)

Video of the real-time measurements displaying nanoantennas at their critical excitation threshold (AVI)

■ AUTHOR INFORMATION

Corresponding Authors

Johannes Schust − *4th Physics Institute and Research Center SCoPE, University of Stuttgart, 70569 Stuttgart, Germany;* orcid.org/0009-0008-8012-5861; Email: johannes.schust@pi4.uni-stuttgart.de

Harald Giessen − *4th Physics Institute and Research Center SCoPE, University of Stuttgart, 70569 Stuttgart, Germany;* Email: giessen@pi4.uni-stuttgart.de

Authors

Florian Mangold − *4th Physics Institute and Research Center SCoPE, University of Stuttgart, 70569 Stuttgart, Germany*

Florian Sterl − *4th Physics Institute and Research Center SCoPE, University of Stuttgart, 70569 Stuttgart, Germany;* orcid.org/0000-0002-1025-6777

Niklas Metz − *4th Physics Institute and Research Center SCoPE, University of Stuttgart, 70569 Stuttgart, Germany*

Thorsten Schumacher − *Experimental Physics III, University of Bayreuth, 95440 Bayreuth, Germany*

Markus Lippitz − *Experimental Physics III, University of Bayreuth, 95440 Bayreuth, Germany;* orcid.org/0000-0003-1218-6511

Mario Hentschel − *4th Physics Institute and Research Center SCoPE, University of Stuttgart, 70569 Stuttgart, Germany*

Complete contact information is available at: https://pubs.acs.org/10.1021/acs.nanolett.3c01070

Author Contributions

#J.S. and F.M. contributed equally.

Notes

The authors declare no competing financial interest.

During publication, we found out that a paper with a very similar topic appeared in Nano Letters.[34]

■ ACKNOWLEDGMENTS

This work was funded by Deutsche Forschungsgemeinschaft (SPP1391 "Ultrafast Nanooptics", SPP1839 "Tailored Disorder", SPP1929 "Giant Interactions in Rydberg Systems"), European Research Council (Advanced Grant ComplexPlas, PoC Grant 3DPrintedOptics), Bundesministerium fr Bildung und Forschung and Carl-Zeiss Stiftung.

REFERENCES

(1) Kauranen, M.; Zayats, A. V. Nonlinear plasmonics. *Nat. Photonics* **2012**, *6*, 737−748.

(2) Aouani, H.; Rahmani, M.; Navarro-Cia, M.; Maier, S. A. Third-harmonic-upconversion enhancement from a single semiconductor nanoparticle coupled to a plasmonic antenna. *Nat. Nanotechnol.* **2014**, *9* (4), 290−294.

(3) Metzger, B.; Hentschel, M.; Schumacher, T.; Lippitz, M.; Ye, X.; Murray, C. B.; Knabe, B.; Buse, K.; Giessen, H. Doubling the efficiency of third harmonic generation by positioning ito nanocrystals into the hot-spot of plasmonic gap-antennas. *Nano Lett.* **2014**, *14*, 2867−2872.

(4) Kravtsov, V.; AlMutairi, S.; Ulbricht, R.; Kutayiah, A. R.; Belyanin, A.; Raschke, M. B. Enhanced third-order optical nonlinearity driven by surface-plasmon field gradients. *Phys. Rev. Lett.* **2018**, *120*, 203903.

(5) Lippitz, M.; van Dijk, M. A.; Orrit, M. Third-harmonic generation from single gold nanoparticles. *Nano Lett.* **2005**, *5*, 799−802.

(6) Ai, Q.; Zhang, H.; Wang, J.; Giessen, H. Multiphoton photoluminescence in hybrid plasmon-fiber cavities with au and au@pd nanobipyramids: Two-photon versus four-photon processes and rapid quenching. *ACS Photonics* **2021**, *8*, 2088−2094.

(7) Lee, J.; Tymchenko, M.; Argyropoulos, C.; Chen, P.-Y.; Lu, F.; Demmerle, F.; Boehm, G.; Amann, M.-C.; Alu, A.; Belkin, M. A. Giant nonlinear response from plasmonic metasurfaces coupled to intersubband transitions. *Nature* **2014**, *511* (7), 65−69.

(8) Metzger, B.; Gui, L.; Fuchs, J.; Floess, D.; Hentschel, M.; Giessen, H. Strong enhancement of second harmonic emission by plasmonic resonances at the second harmonic wavelength. *Nano Lett.* **2015**, *15*, 3917−3922.

(9) Farahani, J. N.; Pohl, D. W.; Eisler, H.-J.; Hecht, B. Single quantum dot coupled to a scanning optical antenna: A tunable superemitter. *Phys. Rev.* **2005**, *95* (6), 17402.

(10) Hentschel, M.; Utikal, T.; Giessen, H.; Lippitz, M. Quantitative modeling of the third harmonic emission spectrum of plasmonic nanoantennas. *Nano Lett.* **2012**, *12* (7), 3778−3782.

(11) Albrecht, G.; Hentschel, M.; Kaiser, S.; Giessen, H. Hybrid organic-plasmonic nanoantennas with enhanced third-harmonic generation. *ACS Omega* **2017**, *2*, 2577−2582.

(12) Hanke, T.; Krauss, G.; Träutlein, D.; Wild, B.; Bratschitsch, R.; Leitenstorfer, A. Efficient nonlinear light emission of single gold optical antennas driven by few-cycle near-infrared pulses. *Phys. Rev.* **2009**, *103* (12), 257404.

(13) Krauth, J.; Giessen, H.; Hentschel, M. Wavelength-dependent third-harmonic generation in plasmonic gold nanoantennas: Quantitative determination of the d-band influence. *ACS Photonics* **2018**, *5*, 1863−1870.

(14) Schumacher, T.; Kratzer, K.; Molnar, D.; Hentschel, M.; Giessen, H.; Lippitz, M. Nanoantenna-enhanced ultrafast nonlinear spectroscopy of a single gold nanoparticle. *Nat. Commun.* **2011**, *2* (5), 333.

(15) Hancu, I. M.; Curto, A. G.; Castro-Lopez, M.; Kuttge, M.; van Hulst, N. F. Multipolar interference for directed light emission. *Nano Lett.* **2014**, *14*, 166−171.

(16) Rybka, T.; Ludwig, M.; Schmalz, M. F.; Knittel, V.; Brida, D.; Leitenstorfer, A. Sub-cycle optical phase control of nanotunnelling in the single-electron regime. *Nat. Photonics* **2016**, *10*, 667−670.

(17) Wolf, D.; Schumacher, T.; Lippitz, M. Shaping the nonlinear near field. Nature Communications. *Nat. Commun.* **2016**, *7* (1), 10361.

(18) Frischwasser, K.; Cohen, K.; Kher-Alden, J.; Dolev, S.; Tsesses, S.; Bartal, G. Real-time sub-wavelength imaging of surface waves with nonlinear near-field optical microscopy. *Nature Photonics 2021 15:6* **2021**, *15*, 442−448.

(19) Hanke, T.; Cesar, J.; Knittel, V.; Trugler, A.; Hohenester, U.; Leitenstorfer, A.; Bratschitsch, R. Tailoring spatiotemporal light confinement in single plasmonic nanoantennas. *Nano Lett.* **2012**, *12*, 992−996.

(20) Aeschlimann, M.; Bauer, M.; Bayer, D.; Brixner, T.; Garcia de Abajo, F. J.; Pfeiffer, W.; Rohmer, M.; Spindler, C.; Steeb, F. Adaptive subwavelength control of nano-optical fields. *Nature* **2007**, *446*, 301−304.

(21) Chen, S.; Li, G.; Zeuner, F.; Wong, W. H.; Pun, E. Y. B.; Zentgraf, T.; Cheah, K. W.; Zhang, S. Symmetry-selective third-harmonic generation from plasmonic metacrystals. *Physical review letters* **2014**, *113*, 33901.

(22) Drechsler, V.; Krauth, J.; Karst, J.; Giessen, H.; Hentschel, M. Switchable optical nonlinearity at the metal to insulator transition in magnesium thin films. *ACS Photonics* **2020**, *7*, 1560−1568.

(23) Krauth, J.; Schumacher, T.; Defrance, J.; Metzger, B.; Lippitz, M.; Weiss, T.; Giessen, H.; Hentschel, M. Nonlinear spectroscopy on the plasmonic analog of electromagnetically induced absorption: revealing minute structural asymmetries. *ACS Photonics* **2019**, *6*, 2850−2859.

(24) Metzger, B.; Hentschel, M.; Lippitz, M.; Giessen, H. Third-harmonic spectroscopy and modeling of the nonlinear response of plasmonic nanoantennas. *Optics letters* **2012**, *37*, 4741−4743.

(25) Wegener, M.; Garcia-Pomar, J. L.; Soukoulis, C. M.; Meinzer, N.; Ruther, M.; Linden, S. Toy model for plasmonic metamaterial resonances coupled to two-level system gain. *Opt. Express* **2008**, *16*, 19785−19798.

(26) Butet, J.; Martin, O. J. F. Evaluation of the nonlinear response of plasmonic metasurfaces: Miller’s rule, nonlinear effective susceptibility method, and full-wave computation. *J. Opt. Soc. Am. B* **2016**, *33* (2), A8−A15.

(27) Steinle, T.; Morz, F.; Steinmann, A.; Giessen, H. Ultra-stable high average power femtosecond laser system tunable from 1.33 to 20m. *Opt. Lett.* **2016**, *41*, 4863.

(28) Dorfmuller, J.; Vogelgesang, R.; Khunsin, W.; Rockstuhl, C.; Etrich, C.; Kern, K. Plasmonic nanowire antennas: Experiment, simulation, and theory. *Nano Lett.* **2010**, *10*, 3596−3603.

(29) Baffou, G.; Quidant, R.; Girard, C. Heat generation in plasmonic nanostructures: Influence of morphology. *Appl. Phys. Lett.* **2009**, *94*, 153109.

(30) Baffou, G.; Quidant, R.; Garcia de Abajo, F. J. Nanoscale control of optical heating in complex plasmonic systems. *ACS Nano* **2010**, *4*, 709−716.

(31) Jauffred, L.; Samadi, A.; Klingberg, H.; Bendix, P. M.; Oddershede, L. B. Plasmonic heating of nanostructures. *Chem. Rev.* **2019**, *119*, 8087−8130.

(32) Shi, L.; Iwan, B.; Nicolas, R.; Ripault, Q.; Andrade, J. R. C.; Han, S.; Kim, H.; Boutu, W.; Franz, D.; Heidenblut, T.; Reinhardt, C.; Bastiaens, B.; Nagy, T.; Babushkin, I.; Morgner, U.; Kim, S.-W.; Steinmeyer, G.; Merdji, H.; Kovacev, M. Self-optimization of plasmonic nanoantennas in strong femtosecond fields. *Optica* **2017**, *4* (9), 1038−1043.

(33) Ko, K. D.; Kumar, A.; Fung, K. H.; Ambekar, R.; Liu, G. L.; Fang, N. X.; Toussaint, K. C. Nonlinear optical response from arrays of au bowtie nanoantennas. *Nano Lett.* **2011**, *11* (1), 61−65.

(34) Schuknecht, F.; Maier, C. M.; Vosshage, P.; Hintermayr, V. A.; Döblinger, M.; Lohmüller, T., Single-Step Plasmonic Dimer Printing by Gold Nanorod Splitting with Light. *Nano Letters* 2023, DOI: 10.1021/acs.nanolett.2c04954.

NOTE ADDED AFTER ASAP PUBLICATION

This paper was published ASAP on May 24, 2023, missing a note about a paper on a similar topic also publishing in Nano Letters. The corrected version was reposted on June 14, 2023.

https://doi.org/10.1021/acs.nanolett.3c01070
Nano Lett. 2023, 23, 5141−5147